

Journal of Materials Chemistry C

Accepted Manuscript



This is an *Accepted Manuscript*, which has been through the Royal Society of Chemistry peer review process and has been accepted for publication.

Accepted Manuscripts are published online shortly after acceptance, before technical editing, formatting and proof reading. Using this free service, authors can make their results available to the community, in citable form, before we publish the edited article. We will replace this *Accepted Manuscript* with the edited and formatted *Advance Article* as soon as it is available.

You can find more information about *Accepted Manuscripts* in the [Information for Authors](#).

Please note that technical editing may introduce minor changes to the text and/or graphics, which may alter content. The journal's standard [Terms & Conditions](#) and the [Ethical guidelines](#) still apply. In no event shall the Royal Society of Chemistry be held responsible for any errors or omissions in this *Accepted Manuscript* or any consequences arising from the use of any information it contains.

Alternated bimetallic [Ru-M] (M = Fe²⁺, Zn²⁺) coordination polymers based on [Ru(bpy)₃]²⁺ units connected to bis-terpyridine ligands : synthesis, electrochemistry and photophysics in solution or in thin film on electrodes.

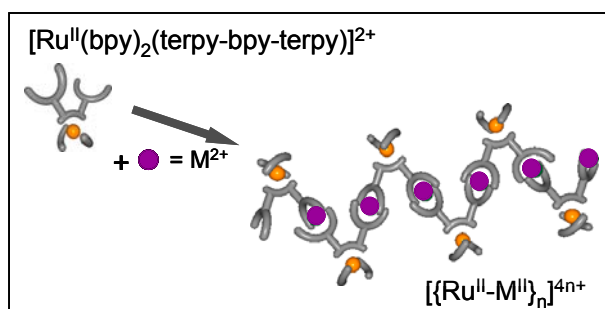
Jean Lombard,^a D. Amilan Jose,^a Carmen E. Castillo,^a Robert Pansu,^b Jérôme Chauvin,^{a*} Alain Deronzier,^{a*} Marie-Noëlle Collomb.^{a*}

^a Université Grenoble Alpes, DCM, F-38000 Grenoble, France
CNRS, DCM, F-38000 Grenoble, France

E-mail: Jerome.chauvin@ujf-grenoble.fr; alain.deronzier@ujf-grenoble.fr; marie-noelle.collomb@ujf-grenoble.fr

^b Ecole Normale supérieure de Cachan / CNRS, Laboratoire de Photophysique et Photochimie Supramoléculaire et Macromoléculaires, UMR-8531, 61 av. du Président Wilson, 94235 Cachan Cedex, France.

Table of contents entry :



A [Ru(bpy)₃]²⁺ like complex bearing two free terpyridine is used to obtain well ordering coordination polymers with photoredox activities.

Abstract.

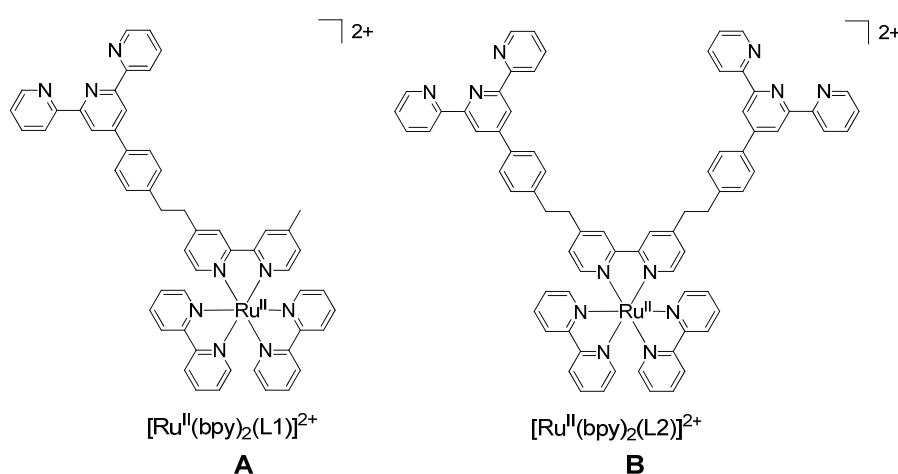
Two alternated bimetallic Ru/Fe and Ru/Zn coordination polymers, $[\{\text{Ru}^{\text{II}}(\text{bpy})_2(\text{L2})\text{M}^{\text{II}}\}_n]^{4n+}$ ($\text{M} = \text{Fe}^{2+}, \text{Zn}^{2+}$), were synthesized using the $[\text{Ru}(\text{bpy})_2(\text{L2})]^{2+}$ ($\text{bpy} = 2,2'$ bipyridine) complex as building block, in which L2 is a bipyridine ligand substituted by two terpyridine sites. The $[\text{Ru}(\text{bpy})_3]^{2+}$ like-subunits provides to the assemblies photoredox properties whereas the second metal allows the build-up of the polymer structure by coordination of the free terpyridine units, associated with additional redox activities. Thin robust films of these metallo supramolecular structures can be easily obtained as coating on electrode surfaces (C, Pt, ITO) by a simple electrochemical procedure based on an electroreductive precipitation adsorption process. The morphology of the films has been characterized by AFM. Electrochemical and photophysical properties of these coordination polymers were investigated in CH_3CN solution as well as thin films deposited on an electrode. The Ru(II)/Zn(II) film, deposited on a transparent ITO electrode, displays luminescence properties. On the other hand, the Ru(II)/Fe(II) film exhibits electrochromic properties under continuous cycling over the $\text{Fe}^{\text{II}}/\text{Fe}^{\text{III}}$ and $\text{Ru}^{\text{II}}/\text{Ru}^{\text{III}}$ waves, shifting from reddish dark at the Fe(II)/Ru(II) reduced state to orange-yellow at the Fe(III)/Ru(II) state and to pale green at the more oxidized state Fe(III)/Ru(III). These oxidation processes can be also driven by visible light. Indeed, upon continuous irradiation of an CH_3CN solution of the Ru/Fe polymer in presence of a diazonium salt as sacrificial electron acceptor, the fast quantitative one-electron oxidation of the Fe(II) centers followed by that of the Ru(II) ones occurs, although the strong quenching of the luminescence of the Ru(II) moieties by the Fe(II) center. The photoinduced oxidation of the Fe(II) center is still efficient when the Ru(II)/Fe(II) polymer is electrodeposited as thin film on ITO leading to the storage of an oxidative equivalent on an electrode.

Introduction

Coordination polymers have attracted a considerable interest in the last ten years because of the great versatility of their fabrication using a simple self-assembling process.¹ By such methodology many, one, two or three dimensional structures has been produced and used as smart material for various applications. The main advantages of these coordination polymers over conventional covalent ones come from the presence of metallic centers providing a wide variety of specific properties as optical, electrical, redox, photochemical, magnetic or catalytical activities. Owing to the large range of available organic ligands and metallic cations, coordination polymers offer a multitude of possibilities to develop intelligent materials with tuneable properties. A specific development in this area concerns the conception of soluble one-dimensional metallopolymers in which the polymeric skeleton is built-up by the *in-situ* formation of a chain of coordination bonds resulting from an alternating incorporation of a metal ion in a polytopic bridging ligand.² Among the most popular ditopic building block ligands those based on polypyridyl, especially 2,2':6',2'' terpyridyl, appear as ideally suitable for the construction of such polymers.³⁻⁷ As a matter of fact the three chelating pyridine groups allows the formation of octahedral metallic complexes having high binding constants and no enantiomers with many metals. The main strategy used consists in the synthesis of a bis-terpyridine ligand in which the two chelating units are covalently connected by a bridging group. Numerous kind of organic bridges (rigid, flexible, conjugated or not, polymeric...) has been investigated, and, depending on the metal used and the flexibility of the bridge linear, oligomers or polymers as well as discrete macrocycles have been obtained.^{2,8-10} Furthermore it has been shown that in general the average molecular weight of the resulting compounds is strongly time, concentration and temperature depending.^{11,12}

More recently this bis-terpyridyl polymer-making technique has been proposed to elaborate more sophisticated nanostructured materials. It consists of using a chemical group having its own specific property, instead of a conventional organic bridge, associated in an alternated mode with the metallic bis-terpyridine one. S. B. Colbran et al. reported one of the first example of such material containing, a rigid diimide bridge as electron acceptor and iron(II) as metal ions.¹² Following this approach strongly fluorescent coordination polymers have been prepared by employing a perylene diimine bridge and Zn^{2+} for the complexation,^{2,14} Zn^{2+} does not interfere with the luminescence and these polymers have been also immobilized on surfaces utilizing a layer by layer technique.^{15,16} Other efficient light-emitting zinc metallopolymers

have been developed based on fluorophore bridge such as fluorene¹⁷⁻¹⁹ or π -conjugated systems.²⁰ In contrast, examples of introduction between the two terminal chelating terpyridine of another metallic complexing site giving to the polymer additional properties, are very rare. Our laboratory made recently a success in this innovative approach by synthesizing a multitopic cyclam bis-terpyridine platform²¹⁻²⁴ from which a series of homo and heterometallic (Cu^{2+} , Fe^{2+} , Co^{2+} and Ni^{2+} ions) coordination polymers has been prepared and characterized. This new class of material exhibits rich properties since two different metal ions can be localized both in the two terpyridine units and in the macrocycle framework. For instance an acid-base driven interconversion between a mononuclear Cu(II) complex and a coordination polymer has been evidenced, while in the presence of Cu(II), Co(II) and Ni(II), redox-responsible polymeric gels are obtained. To continue to explore new tracks in this direction, our idea was how to associate to the bis-terpyridine framework a photoredox sensitizer such as Ru(II) tris(bipyridine), much more convenient than the Ru(II) bis-(terpyridine) system in term of lifetime of the excited state,²⁵ in view to perform efficient photoinduced electron transfer reactions. We previously reported the synthesis of one of the rare examples of heteroditopic ligands containing one 2,2'-bipyridine and one or two 2,2':6',2''-terpyridyl moiety and their Ru(II) tris(bipyridine)-like complexes $[\text{Ru}(\text{bpy})_2(\text{L1})]^{2+}$ and $[\text{Ru}(\text{bpy})_2(\text{L2})]^{2+}$, respectively (Scheme 1).²⁶ We also prepared the corresponding heterobimetallic trinuclear complexes $[\text{M}\{\text{Ru}^{\text{II}}(\text{bpy})_2(\text{L1})\}_2]^{n+}$ with $\text{M} = \text{Fe}^{2+}$, Zn^{2+} , Co^{2+} , Co^{3+} and Mn^{2+} of the single terpyridyl derivative A^{27-31} and fully studied their redox and photophysical behaviour, as well as their capabilities to photoinduce redox reactions in solution.



Scheme 1. Chemical structure of the heteroditopic ligands bearing $[\text{Ru}(\text{bpy})_3]^{2+}$ like moieties we have previously developed.²⁶

We report here the *in-situ* formation of soluble heterometallic coordination polymers, $[\{\text{Ru}^{\text{II}}(\text{bpy})_2(\text{L2})\text{M}^{\text{II}}\}_n]^{4n+}$ (denoted $[\{\text{Ru}^{\text{II}}-\text{M}^{\text{II}}\}_n]^{4n+}$), generated by complexation of Fe^{2+} or Zn^{2+} ions (M^{2+}) with the free terpyridine of $[\text{Ru}(\text{bpy})_2(\text{L2})]^{2+}$ (Scheme 1B) in CH_3CN as well as their electrochemical and photophysical properties. We will show also that robust thin films of these metallo supramolecular structures can be easily achieved on electrode surfaces by a simple electrochemical procedure based on the electroreductive precipitation-adsorption of the polymers, procedure that we previously used for other macromolecular metallic complexes.³²⁻³⁵ Finally we will prove that the polymers can be engaged in photoinduced oxidation processes under visible irradiation in presence of a diazonium salt as sacrificial electron acceptor .

Experimental

Materials and instrumentation. Acetonitrile (CH_3CN , Rathburn, HPLC grade), tetra-*n*-butylammonium perchlorate ($[\text{Bu}_4\text{N}]\text{ClO}_4$, Fluka) and tetra-*n*-butylammonium tetrafluoroborate ($[\text{Bu}_4\text{N}]\text{BF}_4$, Fluka) were used as received and stored under argon in a dry-glovebox (Jaram). 4-Bromophenyl diazonium tetrafluoroborate *p*- $\text{BrC}_6\text{H}_4\text{N}_2(\text{BF}_4)$ (ArN_2^+ ; BF_4^-) (Accros) was used as received. Complex $[\text{Ru}(\text{bpy})_2(\text{L2})](\text{PF}_6)_2$ was synthesized following a procedure already published.²⁶ FeCl_2 (>99%) was purchased from Aldrich and used as received. $\text{Zn}(\text{CF}_3\text{SO}_3)_2$ was prepared from Zn powder following literature.²⁷ The electrospray ionization mass spectrometry (ESI-MS) experiments were performed on a triple quadrupole mass spectrometer Quattro II (Water Micromass). The sampling cone voltage was set to 30 V. Matrix-assisted laser desorption/ionization time-of-flight (MALDI-TOF) mass spectra were recorded on a Bruker-Daltonics Maldi-ToF-ToF Speed. AFM measurements were performed with a Picoplus instrument (Molecular Imaging) equipped with a PicoScan controller and an AC-mode control box. AFM cantilever with an aluminium coating (BudgetSensors Tap150 Al-G) and a nominal spring constant of 5 N m^{-1} was used. Images were treated using Gwyddion program.

Synthesis of $[\{\text{Ru}^{\text{II}}(\text{bpy})_2(\text{L2})\text{Fe}^{\text{II}}\}_n](\text{PF}_6)_{4n}$ denoted $[\{\text{Ru}^{\text{II}}-\text{Fe}^{\text{II}}\}_n]^{4n+}$. To a methanol solution (30 mL) of $[\text{Ru}(\text{bpy})_2(\text{L2})](\text{PF}_6)_2$ (30 mg, 0.0196 mmol), a methanol solution (5 mL) of FeCl_2 (2.5 mg, 0.0196 mmol) was slowly added under inert atmosphere. The resulting solution turned immediately to dark violet and was stirred at RT for 2-3 hrs. Then the volume was reduced under vacuum and a saturated KPF_6 aqueous solution was added, leading to the formation of a dark reddish violet precipitate, which was filtered off, washed with water, diethyl ether and dried under air. Yield: 35 mg (~95%).

Synthesis of $[\{\text{Ru}^{\text{II}}(\text{bpy})_2(\text{L2})\text{Zn}^{\text{II}}\}_n](\text{PF}_6)_{4n}$ denoted $[\{\text{Ru}^{\text{II}}\text{-Zn}^{\text{II}}\}_n]^{4n+}$. To an ethanol solution (30 mL) of $[\text{Ru}(\text{bpy})_2(\text{L2})](\text{PF}_6)_2$ (18 mg, 0.0117 mmol), an ethanol solution (5 mL) of $\text{Zn}(\text{CF}_3\text{SO}_3)_2$ (4.25 mg (0.0117 mmol) was slowly added under inert atmosphere. The orange reaction mixture was heated at reflux for 2-3 hrs under stirring. The resulting solution was cooled at room temperature. Then the volume was reduced under vacuum and a saturated KPF_6 aqueous solution was added, leading to the formation of an orange precipitate, which was filtered off, washed with water, diethylether and dried under air. Yield: 20 mg (~90%)

Absorbance and Emission. UV-visible spectra were obtained using a Cary 1 absorption spectrophotometer and a 1 cm path length quartz cells for polymer in solution. For emission experiments in solution, samples were prepared under Ar in a glove-box and contained in a 1 cm path length quartz cuvette. Samples were maintained under anaerobic conditions with a silicon cap. Emission spectra were recorded at room temperature on a Jobin-Yvon Fluoromax-4. The excitation wavelength was 450 nm. Emission quantum yield ϕ_L were determined at 25°C in deoxygenated acetonitrile solutions with $[\text{Ru}(\text{bpy})_3](\text{PF}_6)_2$ used as a standard ($\phi_L^{\text{ref.}} = 0.062$). Emission lifetime measurements in solution were performed after irradiation at $\lambda = 400$ nm by the second harmonic of Titanium: Sapphire laser. Picoquant Fluotime 200 was used for the decay acquisition. The experiments were performed on the platform “NanoBio Campus” in Grenoble (France). Luminescence decays were analyzed with Fluofit software available from Picoquant. Time-resolved luminescence lifetime experiments on films were performed using a space- and time-correlated photon-counting photomultiplier (Q_A) from Europhoton GmbH mounted onto a microscope.³⁶ The setup was available at laboratoire de Photophysique et Photochimie Supramoléculaire et Macromoléculaire (Cachan-France). The excitation source is an argon-ion laser pumped mode-locked Ti/sapphire laser (Tsunami, by Spectra-Physics) with a pulse-picker and frequency-doubled. Excitation source was 495 nm. The luminescence lifetimes given in this paper correspond to the global emission decay of the analyzed area *i.e.* the decay corresponding to the whole Q_A image.

Electrochemistry. All electrochemical measurements were run under an argon atmosphere in a dry-glovebox at room temperature. Cyclic voltammetry (CV) and controlled potential electrolysis experiments were performed using an EG&G PAR model 173 potentiostat/galvanostat equipped with a PAR model universal programmer 175 and a PAR model 179 digital coulometer. A standard three-electrode electrochemical cell was used.

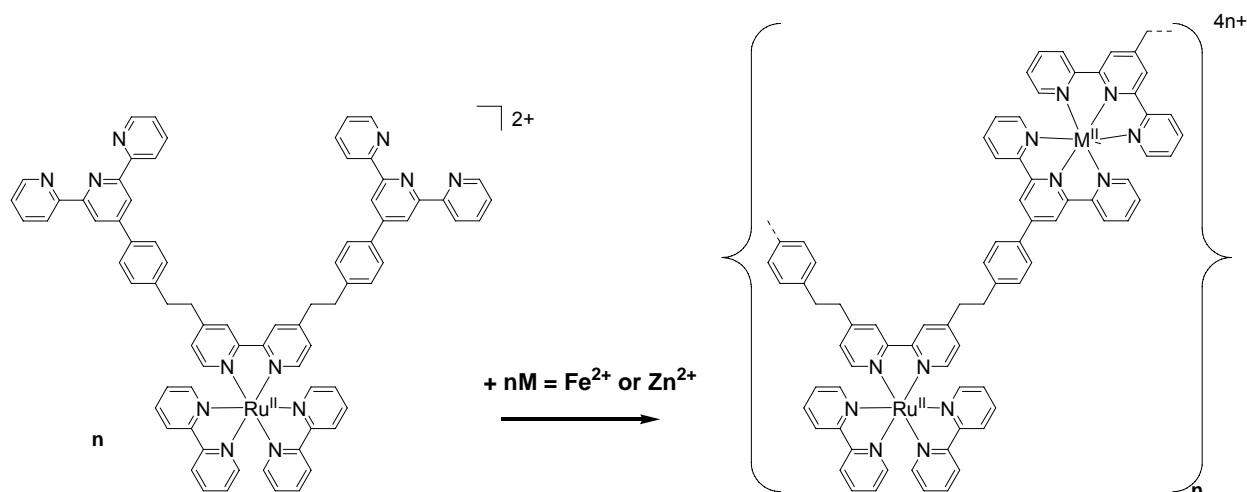
Potentials were referenced to an Ag/10 mM AgNO₃ reference electrode in CH₃CN + 0.1 M [Bu₄N]ClO₄. Potentials referred to that system can be converted to the ferrocene/ferricinium couple by subtracting 87 mV and to SCE or NHE by adding 298 mV or 548 mV, respectively. The working electrode were a 5 mm diameter platinum disk or a 3 mm diameter vitreous carbon electrode polished with 2 μm diamond paste (Mecaprex Presi). Rectangular ITO plates (8 x 25 mm²) were used for the electrodeposition of thin films on transparent support to allow optical characterization. The rotating disk electrode (RDE) was a 2 mm diameter platinum disk with a rotation rate $\omega = 600 \text{ rot min}^{-1}$. The UV-visible spectra of the initial and electrolyzed solutions were transferred to 1 mm path length quartz cuvette cells and were recorded directly in the glovebox with a Cary 50 using optical fibers.

Continuous irradiations. Photoinduced oxidations were performed using a Xe lamp (250 Watt) which UV and IR wavelength were cut off with a UV heatbuster filter (Melles Griot 03MHG101). The samples received around 4.5 mW. For these experiments, all the solutions were prepared in a 1 cm optical cell in dry-glove box under Ar. For the photoinduced oxidation of polymers in solution, the CH₃CN solutions contained a mixture of [$\{\text{Ru}^{\text{II}}\text{-M}^{\text{II}}\}_n\}^{4n+}$] (0.05 mM) and ArN₂⁺ (15 mM). Under these conditions, the concentration of ArN₂⁺ can be considered as constant during the irradiation experiments. For the photoinduced oxidation of [$\{\text{Ru}^{\text{II}}\text{-Fe}^{\text{II}}\}_n\}^{4n+}$] films deposited on ITO, the modified ITO was set in a 1 cm path quartz cuvette in CH₃CN + 0.1 M [Bu₄N]ClO₄ with 15 mM ArN₂⁺, closed with a septum and degassed with argon. Photoinduced oxidation experiments were followed by UV-visible spectroscopy.

Results and Discussion

Synthesis of [$\{\text{Ru}^{\text{II}}\text{-M}^{\text{II}}\}_n\}^{4n+}$] (M = Fe²⁺, Zn²⁺).

The soluble coordination polymers [$\{\text{Ru}(\text{bpy})_2(\text{L}2)\text{M}\}_n\}^{4n+}$] (denoted [$\{\text{Ru}^{\text{II}}\text{-M}^{\text{II}}\}_n\}^{4n+}$]) have been obtained by the addition of one molar equivalent of the metallic ion M²⁺ to a solution of the complex [Ru(bpy)₂(L2)]²⁺. These polymers are self-assembled by coordination of M²⁺ to the terpyridine ligands of the ruthenium complex at room temperature (Scheme 2). They have been prepared in methanol or ethanol solutions by reaction of [Ru(bpy)₂(L2)]²⁺ with FeCl₂ or Zn(CF₃SO₃)₂ and isolated as solid powders by addition of a saturated aqueous solution of KPF₆ (see experimental section). These polymers can be also formed *in situ* in CH₃CN from the metallic ions as perchlorate salt.



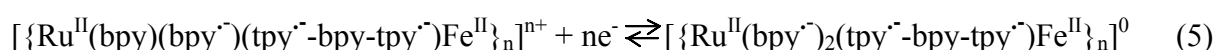
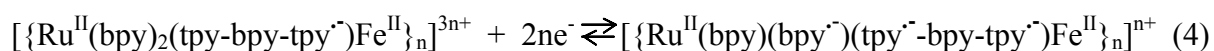
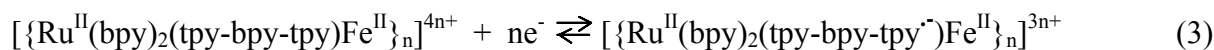
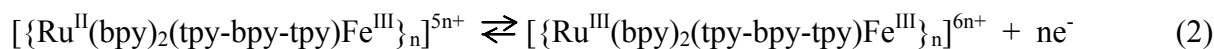
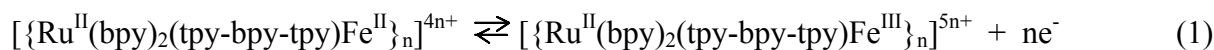
Scheme 2: Chemical formation of $[\{ Ru(bpy)_2(L_2)M \}_n]^{4n+}$ ($M = Fe, Zn$).

Solutions of isolated or *in situ* prepared polymers were found to exhibit identical UV-Visible absorption and electrochemical characteristics. Isolated $[\{ Ru^{II}-Fe^{II} \}_n]^{4n+}$ polymer was characterized by electrospray ionization (ESI) and MALDI-TOF mass spectroscopies. ESI-MS spectra shows the Ru-Fe monomeric base peak $[M-PF_6]^+$ ($M = [Ru(bpy)_2(L_2)Fe](PF_6)_4$) at m/z 480.5 and the $[Ru(bpy)_2(L_2)]^{2+}$ entity at m/z 620.1 (Figure SI1). Several multi-charged peaks related to dimeric units were also observed. The MALDI-TOF mass spectroscopy (Figure SI2) provides support for the formation of coordination polymers. Indeed, in the m/z range of 3000 to 12000, different distributions corresponding to the mass of oligomers of up to five repeated Ru-Fe monomeric units were detected. The characteristic signals for oligomers observed are spaced regularly and can be associated with the addition of the base peak (M). In addition, the intensity of the signals decreases as the molecular weight increases, feature frequently observed in the MALDI-TOF spectra of polymers, because the intensity depends on the ability of the molecule to reach the detector. Therefore, the presence of structures of higher molecular weight in solution is also likely.³⁷

Electrochemistry in solution.

The redox properties of the building block $[Ru^{II}(bpy)_2(L_2)](PF_6)_2$ complex are described in supplementary informations (Figure SI3, Table SI1). The cyclic voltammogram (CV) of $[\{ Ru^{II}-Fe^{II} \}_n]^{4n+}$, in CH_3CN containing 0.05 M $[Bu_4N]BF_4$, is actually the sum of electroactivity of both metallic subunits, the Fe^{II} -bis-terpyridine and the Ru^{II} -tris-bipyridine, in accordance with the absence of an electronic connection between the metallic centres. In the positive potential

region, the two well-separated reversible oxidation systems observed at $E_{1/2} = +0.75$ and $+0.91$ V are thus readily assigned to the $\text{Fe}^{\text{III}}/\text{Fe}^{\text{II}}$ and $\text{Ru}^{\text{III}}/\text{Ru}^{\text{II}}$ redox couples, respectively (eqs. (1, 2)) (Table 1, Figures 1 and SI4). Moreover, rotating disk electrode (RDE) experiments confirm that the macromolecular structure is maintained in solution, since the height of the ruthenium wave and that of iron are similar, in accordance with the 1:1 Ru/Fe stoichiometry (Figure 1C). In the negative region, the CV exhibits a series of ligand centred reduction processes, more or less reversible. Reduction processes are readily attributed by comparison with the trinuclear complex $[\{\text{Ru}^{\text{II}}(\text{bpy})_2(\text{L1})\}_2\text{Fe}^{\text{II}}]^{6+}$.²⁷ The first one, located at $E_{1/2} = -1.52$ V, corresponds to the reduction of one terpyridine ligand of the Fe(II) unit (eq. (3)). The second system ($E_{1/2} = -1.61$ V), distorted by adsorption phenomena, is associated to the simultaneous reduction of the second terpyridine ligand coordinated to the Fe(II) and the reduction of one bipyridine of the Ru(II) center (a bipyridine not connected to the terpyridine) (eq. (4)). The third one ($E_{1/2} = -1.80$ V) is due to the reduction of the second bipyridine of the Ru(II) units (eq. (5)). The fourth system ($E_{1/2} = -2.20$ V) is related to the reduction of the bipyridine of the heteroditopic ligand (eq. (6)).



Both oxidized forms of $[\{\text{Ru}^{\text{II}}\text{-Fe}^{\text{II}}\}_n]^{4n+}$, *i.e.* $[\{\text{Ru}^{\text{II}}\text{-Fe}^{\text{III}}\}_n]^{5n+}$, and $[\{\text{Ru}^{\text{III}}\text{-Fe}^{\text{III}}\}_n]^{6n+}$, are stable and are generated by two successive electrolyses carried out, respectively, at $+0.90$ and $+1.05$ V with a 95 % yield, as quantified by RDE experiments (Figure 1B). Taking into account the large difference of potential between the $\text{Fe}^{\text{III}}/\text{Fe}^{\text{II}}$ and $\text{Ru}^{\text{III}}/\text{Ru}^{\text{II}}$ redox processes (Table 1), the mixed valent species $[\{\text{Ru}^{\text{II}}\text{-Fe}^{\text{III}}\}_n]^{5n+}$ is perfectly stable. The two oxidized forms $[\{\text{Ru}^{\text{II}}\text{-Fe}^{\text{III}}\}_n]^{5n+}$ and $[\{\text{Ru}^{\text{III}}\text{-Fe}^{\text{III}}\}_n]^{6n+}$ are identified by their visible absorption spectrum (Figure 2). Absorption spectrum of $[\{\text{Ru}^{\text{II}}\text{-Fe}^{\text{II}}\}_n]^{4n+}$ closely results from the overlap of the two parents subunits (Table 2). The two bands at 455 and 568 nm are attributed respectively to the $\text{Ru}(\text{II}) \rightarrow \text{bpy}$ and $\text{Fe}(\text{II}) \rightarrow \text{terpy}$ MLCT. The bands in the UV part of the spectrum are due to the $\pi \rightarrow \pi^*$ transitions of the ligands. After one electron per complex has been passed at $+0.90$ V, the

initial band of the Fe(II) unit at 568 nm disappears on behalf of the appearance of a shoulder around 390 nm and a low intensity band centered at 670 nm typical of the Fe(III) species (Figure 2). The slight loss of intensity of the Ru(II) visible band ($\lambda_{\text{max}} = 454$ nm) is due to the lower absorbance of the Fe(III) unit compared to Fe(II) in this wavelength region. After exchange of one additional electron at +1.05 V, the band of the Ru(II) units at 455 nm disappears and is replaced by those of the Ru(III) ones (shoulder around 430 nm and a slight increase of the band around 660 nm).²⁷ A back electrolysis of the $[\{\text{Ru}^{\text{III}}\text{-Fe}^{\text{III}}\}_n]^{6n+}$ solution at +0.60 V fully regenerates $[\{\text{Ru}^{\text{II}}\text{-Fe}^{\text{II}}\}_n]^{4n+}$. The reaction is controlled by UV-visible (Figure 2) and CVs (not shown). The CV of $[\{\text{Ru}^{\text{II}}\text{-Zn}^{\text{II}}\}_n]^{4n+}$, in the negative potential region, is very similar to that of $[\{\text{Ru}^{\text{II}}\text{-Fe}^{\text{II}}\}_n]^{4n+}$ (Figure SI5). The ligand centred reduction processes are also located at similar potentials (Table 1), attesting that the Zn^{2+} ion is coordinated to two terpyridine ligands. In the positive potential region, as expected, only the $\text{Ru}^{\text{III}}/\text{Ru}^{\text{II}}$ oxidation system is observed at $E_{1/2} = +0.91$ V. Since, the Zn(II)-bis-terpyridine center does not absorb in the visible, the visible absorption spectrum of $[\{\text{Ru}^{\text{II}}\text{-Zn}^{\text{II}}\}_n]^{4n+}$ is similar to that of $[\text{Ru}(\text{bpy})_2(\text{L2})]^{2+}$ and exhibits only the characteristic MLCT absorption band of the Ru(II) units at 455 nm (Table 2).

Elaboration of modified electrodes.

As previously observed for a solution of $[\text{Fe}^{\text{II}}(\text{Ln})_{3/2}]_m^{2m+}$,³² or $[\text{Fe}^{\text{II}}(\text{chir})_{3/2}]_m^{2m+}$,³³ (where Ln is a bis-bipyridine and chir a chiral bis-(pinene-bipyridine) type ligand) a rapid film growth of $[\{\text{Ru}^{\text{II}}\text{-Fe}^{\text{II}}\}_n]^{4n+}$ on Pt, C or ITO electrodes occurs by continuously cycling over the three reduction systems. Figure 3 shows the formation of the $[\{\text{Ru}^{\text{II}}\text{-Fe}^{\text{II}}\}_n]^{4n+}$ thin film on a Pt electrode, in a potential range including the three first reduction systems. The three waves grow in and have a respective potential which correspond closely to the potential observed in solution for the soluble species $[\{\text{Ru}^{\text{II}}\text{-Fe}^{\text{II}}\}_n]^{4n+}$. If the potential range includes only the two first reduction waves the film deposition occurs with a lower efficiency. By cycling only on the first one, the film deposition is not efficient. If the repeated scans are limited on the $\text{Fe}^{\text{II}}/\text{Fe}^{\text{III}}$ and $\text{Ru}^{\text{II}}/\text{Ru}^{\text{III}}$ reversible oxidation waves, no deposition is observed. After ten successive cycles including the three reduction systems, the apparent surface coverage (Γ in mol cm^{-2}) of electroactive species immobilised, after transfer of the electrode into polymer-free CH_3CN , 0.1 M $[\text{Bu}_4\text{N}]\text{ClO}_4$ solution (see below), is of about 6.3×10^{-9} mol cm^{-2} . The Pt/ $[\{\text{Ru}^{\text{II}}\text{-Fe}^{\text{II}}\}_n]^{4n+}$ modified electrode exhibits the same basic electrochemical behaviour as in solution. If the Pt electrode is replaced by a transparent ITO, similar behavior is obtained with a deposition of a film on electrode by cycling on the first three reduction system of the ligands (Figure SI6). UV-

visible spectrum clearly reveals the deposition of the dark reddish film with the characteristic MLCT absorption bands of the Ru(II) and Fe(II) subunits in the visible at 450 and 573 nm respectively (Figure 4). The maximum absorption wavelength of the Fe(II) center is only slightly red-shifted compared to the solution. All these experiments indicate that the origin of the film formation is the poor solubility of the doubly reduced forms of the oligomeric species, *i.e.* $[\{\text{Ru}^{\text{II}}(\text{bpy}^{\cdot-})_2(\text{tpy}^{\cdot-}\text{-bpy-tpy}^{\cdot-})\text{Fe}^{\text{II}}\}_n]^0$ (eq. 5), inducing their strong adsorption (after precipitation) on the electrode surface. It should be noted that such electrodeposition phenomenon was not observed for the trinuclear complexes $[\{\text{Ru}^{\text{II}}(\text{bpy})_2\text{L1}\}_2\text{M}]^{n+}$ ($\text{M} = \text{Fe}^{2+}$, Zn^{2+} , Co^{2+} , Co^{3+} and Mn^{2+})²⁷⁻³¹ by similar reductive scanning. This confirms unambiguously the macromolecular nature of the *in situ* formed species. A similar film formation by electroreductive precipitation-adsorption was previously observed for hydrophobic Ru(II) tris-bipyridine complexes where one, two or three bpy ligand are linked to polypyrrole groups through a long (C13) alkyl chain.^{34, 35} In such cases, the reductive electrodeposition is effective either from these soluble monomeric complexes or from their soluble corresponding polymers. Interestingly, the $[\{\text{Ru}^{\text{II}}\text{-Fe}^{\text{II}}\}_n]^{4n+}$ modified electrodes exhibit toward electrochemical cycling between the Fe(II)-Ru(II) and Fe(III)-Ru(III) states an excellent stability, comparable to that obtained with a polypyrrole³⁴ or polyvinyl³⁸ backbone. About 8% loss of integrated peak current is typically observed after 20 cycles at 100 mV s⁻¹ between 0 and +1.0 V while the intensity of the signal remains almost constant for 80 subsequent anodic scans (less than 10% loss). Films are less stable towards multiple reductive scans.

In addition, during continuous cycling between +0.6 and +1.5 V, the film shows multi-color electrochromic properties as it was recently reported with a Ru(II)-Fe(II) polymer built with bis-terpyridine ligand.⁶ At a starting potential of +0.6 V, the film is reddish brown with a large absorption in the visible at 450 and 573 nm for the Ru(II) and Fe(II) subunits, respectively (see above) (Figure 4). When the potential is increased up to +1.5 V, the visible absorbance decreases in two steps. First, the band centered at 573 nm progressively disappears due to the oxidation of Fe(II) to Fe(III). At about +1.0V the Fe(II) centers are all oxidized and the film becomes orange-yellow. At higher potential the Ru(II) centers are oxidized to Ru(III) and the band centered at 450 nm decreases until its complete disappearance. At +1.5 V the film turns to pale green (Figure 4). Thin films of $[\{\text{Ru}^{\text{II}}\text{-Zn}^{\text{II}}\}_n]^{4n+}$ can be also deposited on Pt, C or transparent ITO electrodes surface in the same conditions that those used for the growth of $[\{\text{Ru}^{\text{II}}\text{-Fe}^{\text{II}}\}_n]^{4n+}$ films (Figure SI7). In this case the films exhibit a yellow coloration and the

UV-visible spectrum after electro-deposition on ITO exhibits only the characteristic MLCT absorption band of the Ru(II) units at 465 nm (Figure SI8A).

AFM measurements on ITO modified $[\{\text{Ru}^{\text{II}}\text{-Fe}^{\text{II}}\}_n]^{4n+}$ and $[\{\text{Ru}^{\text{II}}\text{-Zn}^{\text{II}}\}_n]^{4n+}$ electrode were performed in tapping mode in order to study the surface morphologies and to determine the thickness of the films. Figure 5 shows topography of naked ITO electrode and a $[\{\text{Ru}^{\text{II}}\text{-Fe}^{\text{II}}\}_n]^{4n+}$ modified electrode with a surface coverage value estimated to $\Gamma = 5.83 \cdot 10^{-8} \text{ mol cm}^{-2}$. The ITO electrode presents a homogenous granular topology with a root mean square roughness r.m.s. of 2.57 nm (Figure 5A). After electrodeposition of the $[\{\text{Ru}^{\text{II}}\text{-Fe}^{\text{II}}\}_n]^{4n+}$ film, the topography appears nodular, in homogeneous, typical of an electrodeposited film³⁹ (Figure 5B) and the roughness value increases significantly to 160.4 nm. In order to determine the film thickness, the modified electrode was scratched with a needle and the difference of altitude between the free ITO surface and the deposited film was measured in the tapping mode. The thickness is estimated to 300 nm. As expected, films of thinner thickness can be obtained when the number of repeated potential scans for electrodeposition is reduced, resulting in a lower Γ values.⁴⁰

Emission properties.

Steady state and time-resolved emission of $[\{\text{Ru}^{\text{II}}\text{-M}^{\text{II}}\}_n]^{4n+}$ were recorded in deoxygenated CH_3CN solution and also as a thin film electro-deposited on ITO. Upon excitation at 450 nm, solutions of $[\{\text{Ru}^{\text{II}}\text{-M}^{\text{II}}\}_n]^{4n+}$ exhibit luminescence properties typical of the Ru(II)-tris-bipyridine subunits (Table 2). Emission quantum yield of $[\{\text{Ru}^{\text{II}}\text{-Zn}^{\text{II}}\}_n]^{4n+}$ remains similar to that of the monomer $[\text{Ru}(\text{bpy})_2(\text{L}2)]^{2+}$. By contrast, the emission quantum yield of $[\{\text{Ru}^{\text{II}}\text{-Fe}^{\text{II}}\}_n]^{4n+}$ is drastically lowered and represents only 4% of the emission of $[\{\text{Ru}^{\text{II}}\text{-Zn}^{\text{II}}\}_n]^{4n+}$. This strong luminescence inhibition of the Ru(II) center by the Fe(II) core is comparable to the process occurring within the corresponding trinuclear complex $[\{\text{Ru}(\text{bpy})_2(\text{L}1)\}_2\text{Fe}]^{6+}$ and is attributed to an energy transfer (En.T.) process.^{27,41} Luminescence intensity decay $I(t)$ of solutions of both polymers can be fitted by a bi-exponential function following equation (7)

$$I(t) = A \exp\left(-\frac{t}{\tau_1}\right) + (1 - A) \exp\left(-\frac{t}{\tau_2}\right) \quad (7)$$

where τ_1 and τ_2 are respectively the short and long lifetime component of the decay and A the fraction of emitted intensity associated with τ_1 (Table 2). Figure 6 shows the typical emission decay of $[\{\text{Ru}^{\text{II}}\text{-Zn}^{\text{II}}\}_n]^{4n+}$ in CH_3CN . Bi-exponential decay was already observed for the emission of the trinuclear complex $[\{\text{Ru}(\text{bpy})_2(\text{L}1)\}_2\text{Fe}]^{6+}$ and attributed to quenched and

unquenched $[\text{Ru}(\text{bpy})_3]^{2+}$ unit by the $[\text{Fe}(\text{terpy})_2]^{2+}$ core;^{27, 30, 42} emission decay of the trinuclear complex $[\{\text{Ru}(\text{bpy})_2(\text{L1})\}_2\text{Zn}]^{6+}$ is, on the other hand, simple exponential, with a lifetime close to that of $[\text{Ru}(\text{bpy})_3]^{2+}$.³⁰ The bi-exponential decay of $[\{\text{Ru}^{\text{II}}-\text{Zn}^{\text{II}}\}_n]^{4n+}$ can thus be the result of the polymer structure and may be due to some self quenching process between the excited state of the Ru(II) centers located in a close environment as a consequence of the folding of the polymer chain. Multi-exponential luminescence decay for polymers bearing coordination complexes as emitting centers is a common behavior that was already observed for instance with $[\text{Ru}(\text{bpy})_3]^{2+}$ like complexes as pendant group of polystyrene⁴³ or polypyrrole⁴⁴ backbone. Such decay has been also observed when coordination complexes are part of the polymer backbone as with $[\text{Re}(\text{CO})_2(\text{bpy})\text{PP}]_n$ polymer where PP is a bidentate phosphorus ligand.⁴⁵ This phenomenon is usually attributed to energy migration between adjacent photosensitizers. The quenching rate constant (k_q) occurring in $[\{\text{Ru}^{\text{II}}-\text{M}^{\text{II}}\}_n]^{4n+}$ can be calculated according to equation (8):

$$k_q = \frac{1}{\tau_1} - \frac{1}{\tau_2} \quad (8)$$

k_q are respectively estimated to $3.1 \times 10^8 \text{ s}^{-1}$ and $6.7 \times 10^7 \text{ s}^{-1}$ for $[\{\text{Ru}^{\text{II}}-\text{Fe}^{\text{II}}\}_n]^{4n+}$ and $[\{\text{Ru}^{\text{II}}-\text{Zn}^{\text{II}}\}_n]^{4n+}$. This shows that the quenching rate constant of Ru(II)* by a Fe(II) center is more efficient than the desactivation of Ru(II)* by spatially close Ru(II) center in $[\{\text{Ru}^{\text{II}}-\text{Zn}^{\text{II}}\}_n]^{4n+}$. For $[\{\text{Ru}^{\text{II}}-\text{Fe}^{\text{II}}\}_n]^{4n+}$, k_q falls in the same range than for the processes occurring in the trinuclear $[\{\text{Ru}(\text{bpy})_2(\text{L1})\}_2\text{Fe}]^{6+}$ complex ($k_q = 2 \times 10^8 \text{ s}^{-1}$).²⁷

$[\{\text{Ru}^{\text{II}}-\text{M}^{\text{II}}\}_n]^{4n+}$ have both been electrodeposited on ITO electrode following the procedure describe in the previous section. ITO/ $[\{\text{Ru}^{\text{II}}-\text{Fe}^{\text{II}}\}_n]^{4n+}$ thin films are poorly luminescent, and their emission properties remains difficult to analyse properly with our experimental set-up. Emission of an ITO/ $[\{\text{Ru}^{\text{II}}-\text{Zn}^{\text{II}}\}_n]^{4n+}$ thin film was however detectable with a maximum emission wavelength at around 595 nm after excitation at 450 nm (Figure SI8B).

The luminescent decay of the film recorded upon excitation at 343 nm is multiexponential and best fitted in the first 80 ns by a stretched exponential function (eq. (9)) (Figure 7).

$$I(t) = A \exp\left[-\left(\frac{t}{\tau}\right)^\beta\right] + C \quad (9)$$

The stretching exponent β is estimated to 0.40. This low value suggests a large distribution of exponential to describe the luminescence decay of the Ru(II)* centers in the film and reflects a disordered and heterogeneous media, with several desactivation pathways via self quenching, triplet-triplet annihilation or by the ITO surface itself. The Ru(II)* centres should be considered

as located in different microenvironment. An average relaxation time τ_0 of 31 ns is found according to equation 10

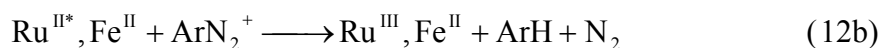
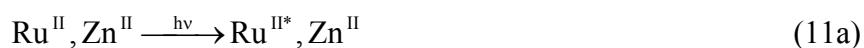
$$\tau_0 = \frac{\tau}{\beta} \Gamma\left(\frac{1}{\beta}\right) \quad (10)$$

Five different electrodeposited films show all a very homogeneous surface coverage with emission relaxation times ranging from 29 to 35 nanoseconds. Spots exhibiting under irradiation the stronger emission intensity possess the shorter luminescence relaxation time (Figure 8 and SI9). Photoluminescent Zn(II) and Fe(II) coordination oligomers and polymers were already obtained from bis-terpyridine containing a perylene bisimide^{2,14} or fluorene⁴⁶ building blocks. The Zn(II) supramolecular architectures are more emissive in solution than our bimetallic systems, with quantum yield up to 85% if a perylene bisimide derivative is used as fluorophore.¹⁴ Their luminescence lifetime estimated around 4 ns in DMF¹⁴ and to less than 1 ps for film constructed following a layer-by-layer fabrication on surface¹⁵ are drastically shorter than our bimetallic polymers. These short excited state lifetimes would limit the application of such assemblies for photoredox process, in contrast to our system, especially when polymers are coated on surface.

Photoredox behaviour.

The $[\{\text{Ru}^{\text{II}}-\text{M}^{\text{II}}\}_n]^{4n+}$ polymers solubilized in CH_3CN solution can be photooxidized under visible light irradiation, in the presence of an irreversible electron acceptor such as 4-bromophenyl diazonium salt (ArN_2^+). We have already proved the efficient photogeneration of $[\text{Ru}^{\text{III}}(\text{bpy})_3]^{3+}$ via the photoinduced electron transfer process between $[\text{Ru}(\text{bpy})_3]^{2+*}$ and ArN_2^+ . This reaction is highly favourable with a ΔG estimated to around -0.67 V, and a large quantum yield of 0.34.^{47,48} In the presence of $[\text{Fe}(\text{terpy})_2]^{2+}$, since the photogenerated Ru(III) is a good oxidant toward the Fe(II) center ($\Delta G = -0.22\text{V}$), continuous irradiation induced the formation of both Fe(III) and Ru(III) centers when ArN_2^+ is added in large excess.²⁷ Similar photoinduced oxidation processes have been obtained for the polymer structures, $[\{\text{Ru}^{\text{II}}-\text{Zn}^{\text{II}}\}_n]^{4n+}$ and $[\{\text{Ru}^{\text{II}}-\text{Fe}^{\text{II}}\}_n]^{4n+}$. Equations (11, 12) summarize the overall photooxidation processes for both compounds. Continuous irradiation of a mixture of $[\{\text{Ru}^{\text{II}}-\text{Zn}^{\text{II}}\}_n]^{4n+}$ with ArN_2^+ (15 mM) in CH_3CN induces the photogeneration of the Ru(III) center as evidenced by the decrease of the MLCT band of Ru(II) unit at 455 nm and the concomitant increase of the LMCT band of Ru(III) at 660 nm with a shoulder at 430 nm (Figure 9) (eqs. (11a, b)). The evolution of UV-visible spectra of $[\{\text{Ru}^{\text{II}}-\text{Fe}^{\text{II}}\}_n]^{4n+}$ under irradiation with ArN_2^+ shows the expected two-step

formation of the Fe(III) and the Ru(III) centers (Figure 10) and resemble those obtained during the electrochemical oxidation (Figure 2). In the first step (Figure 10A), in accordance with the formation of $[\{\text{Ru}^{\text{II}}\text{-Fe}^{\text{III}}\}_n]^{5n+}$ through the transient photogenerated Ru(III) species (eqs. 12a-c), the band of the Fe(II) unit at 568 nm decreases regularly until to almost disappear totally, at the expense of the progressive emergence of a shoulder around 390 nm and a band centred at 670 nm typical of the Fe(III) species. A prolonged irradiation induces, in a second step (Figure 10B), the formation of $[\{\text{Ru}^{\text{III}}\text{-Fe}^{\text{III}}\}_n]^{6n+}$ illustrates by the decrease of the MLCT band of Ru(II) and the slight increase of the band centered at 660 nm (eqs. (12 d, e)).



Quantitative oxidation of the Ru(II) centers into the $[\{\text{Ru}^{\text{II}}\text{-Zn}^{\text{II}}\}_n]^{4n+}$ (eqs. (11 a, b)) and of the Fe(II) centers into the $[\{\text{Ru}^{\text{II}}\text{-Fe}^{\text{II}}\}_n]^{4n+}$ (eqs. (12 a-c)) proceeds in a close time range. The kinetics is slightly slower for the $[\{\text{Ru}^{\text{II}}\text{-Fe}^{\text{II}}\}_n]^{4n+} \rightarrow [\{\text{Ru}^{\text{II}}\text{-Fe}^{\text{III}}\}_n]^{5n+}$ photoinduced transformation as a probable consequence of the En.T. process between the Ru(II)* and Fe(II) centers, which competes with the PET. Surprisingly the quantitative oxidation of the Ru(II) centers into the $[\{\text{Ru}^{\text{II}}\text{-Fe}^{\text{III}}\}_n]^{5n+}$ structure (eqs. (12 d, e)) is almost 10 times slower under similar irradiation conditions. The more oxidized $[\{\text{Ru}^{\text{II}}\text{-Fe}^{\text{III}}\}_n]^{5n+}$ polymer seems to alter the efficient photoinduced oxidation of the Ru(II) subunits. Photo-oxidation kinetics rate constant of Ru(II) subunits by ArN_2^+ depend on the Stern-Volmer constant and on the average luminescence lifetime of the Ru(II)* centers. To investigate the reason of such difference, Stern-Volmer experiments have been conducted between $[\{\text{Ru}^{\text{II}}\text{-Fe}^{\text{II}}\}_n]^{4n+}$ and ArN_2^+ on one hand and $[\{\text{Ru}^{\text{II}}\text{-Fe}^{\text{III}}\}_n]^{5n+}$ on the other hand; $[\{\text{Ru}^{\text{II}}\text{-Fe}^{\text{III}}\}_n]^{5n+}$ being prepared by an exhaustive electrolysis of $[\{\text{Ru}^{\text{II}}\text{-Fe}^{\text{II}}\}_n]^{4n+}$ at 0.8V. The Stern-Volmer constants (K_{SV}) are respectively estimated to 350 and 560 M^{-1} and cannot explain fully the difference of kinetics for the two steps of Figure 10, which may also result in a difference in the average luminescence lifetime of Ru(II)* subunits in both $[\{\text{Ru}^{\text{II}}\text{-Fe}^{\text{II}}\}_n]^{4n+}$ and $[\{\text{Ru}^{\text{II}}\text{-Fe}^{\text{III}}\}_n]^{5n+}$.

Finally the photoinduced oxidation processes of the metallic centers has been also investigated on a $[\{\text{Ru}^{\text{II}}\text{-Fe}^{\text{II}}\}_n]^{4n+}$ film electrodeposited on an ITO electrode. In that case, the temporal

evolution of the UV-visible spectra under irradiation shows the disappearance of the absorption band at 573 nm and an increase of the absorption in the UV part which can be attributed to the generation of Fe(III) centers (figure 11). In spite of the efficient energy transfer process that almost switch off the luminescence of the Ru(II) centers in the $[\{\text{Ru}^{\text{II}}\text{-Fe}^{\text{II}}\}_n]^{4n+}$ film, PET can still occur at the interface of the film and the solution. It generates Fe(III) centers following equations 12 a-c. When the film is removed from the cuvette, visual examination shows that it turns from reddish to orange. On the other hand, the solution used to photooxidized the film turns to pale yellow and a UV-visible spectrum of the solution indicates that a small amount of $[\{\text{Ru}^{\text{II}}\text{-Fe}^{\text{III}}\}_n]^{5n+}$ is dissolved in the solution after 10 min of irradiation. Thus, irradiation causes some desorption of the thin polymer film from the ITO surface. At ambient, the orange $[\{\text{Ru}^{\text{II}}\text{-Fe}^{\text{III}}\}_n]^{5n+}$ film is slowly reduced into $[\{\text{Ru}^{\text{II}}\text{-Fe}^{\text{II}}\}_n]^{4n+}$ and turns back to its initial reddish color.

Conclusion.

We report in this paper, the easy obtention of alternated bimetallic Ru(II)/M(II) ($M = \text{Fe}^{2+}$, Zn^{2+}) coordination polymers from a $[\text{Ru}(\text{bpy})_3]^{2+}$ derivative bearing two free terpyridine coordination sites on one bipyridine. These coordination polymers represent the first example of this kind of photoactive polymers. These coordination polymers are soluble in CH_3CN and exhibit photoactivities. For instance they can be photooxidized under visible light in presence of a diazonium salt acting as sacrificial electron acceptor. Another interesting property is their easy deposition on an electrode surface as photoredox active films via a simple electrodeposition technique which is based on repetitive scans on the ligand-centered reduction processes. Electro- and photo-activable thin films of different thickness were readily obtained by this electrochemical method. The Ru(II)/Fe(II) film deposited on a transparent ITO electrode exhibits electrochromic properties under continuous cycling over the $\text{Fe}^{\text{II}}/\text{Fe}^{\text{III}}$ and $\text{Ru}^{\text{II}}/\text{Ru}^{\text{III}}$ oxidation waves, shifting from reddish dark at the Fe(II)/Ru(II) reduced state to orange-yellow at the Fe(III)/Ru(II) state and to pale green at the more oxidized state Fe(III)/Ru(III). On the other hand, the Ru(II)/Zn(II) film displays luminescence properties with average lifetime around 30 ns. Besides, the emission of the $[\text{Ru}(\text{bpy})_3]^{2+}$ subunit is almost totally quenched in the Ru(II)/Fe(II) polymers. Despite the strong inhibition of the excited state lifetime, the Ru(II)/Fe(II) film exhibits also photoredox activities that allow its photo-oxidation. This study shows that the approach we developed here is attractive for producing soluble as well as thin films of photoactive based $[\text{Ru}(\text{bpy})_3]^{2+}$ coordination polymer functionalized by another metallic complex. Work is in progress in our laboratory to design new polymer structures coupling photosensitive and catalytic properties using this strategy.

Supporting Information Available. Electrochemical behaviour of $[\text{Ru}(\text{bpy})_2(\text{L}2)]^{2+}$, $[\{\text{Ru}^{\text{II}}-\text{Fe}^{\text{II}}\}_n]^{4n+}$ and $[\{\text{Ru}^{\text{II}}-\text{Zn}^{\text{II}}\}_n]^{4n+}$, absorption and emission of $[\{\text{Ru}^{\text{II}}-\text{Zn}^{\text{II}}\}_n]^{4n+}$ on ITO.

Acknowledgements

The authors thank the Agence Nationale pour la Recherche (Grant No. ANR-05-JCJC-0171-01 (Polycomsa) and the LabEx ARCANÉ (ANR-11-LABX-0003-01) for financial support. This work was also supported by ICMG FR 2607 from the chemistry platform «NanoBio campus» in Grenoble, on which MALDI-TOF, AFM and luminescence lifetime measurement in solution has been performed. A. J. and C. E. C. thank the DCM UJF/CNRS UMR 5250 for financial support. Pr Jean-Claude Leprêtre and Dr. Damien Jouvenot are gratefully thanked for their assistance in ligand synthesis.

References:

- ¹ For recent reviews see for instance : a) N.N. Adarsh, P. Dastidar, *Chem. Soc. Rev.*, 2012, **41**, 3039-3060; b) A. S. Abd-El-Aziz, E. A. Strohm, *Polymer*, 2012, **53**, 4879-4921; c) E. C. Constable in coordination polymer , P.A. Gale, J.W. Steed Ed. *Supramolecular chemistry : from molecules to nanomaterials*, 2012, **6**, 3073-3086, J. Wiley and Sons Ltd., Chichester, UK
- ² R. Dobraza, M. Lysetska, P. Ballester, M. Grune, F. Würthner, *Macromolecules*, 2005, **38**, 1315-1325.
- ³ E. C. Constable, A. Thompson, *J. Chem. Soc., Dalton Trans.*, 1992, 3467-3475.
- ⁴ E. C. Constable, *Macromol. Symp.*, 1995, **98**, 503-524
- ⁵ A. Wild, A. Winter, F. Schlütter, U. S. Schubert, *Chem. Soc. Rev.*, 2011, **40**, 1459-1511.
- ⁶ C.-W. Hu, T. Sato, J. Zhang, S. Moriyama, M. Higuchi, *J. Mater. Chem. C.*, 2013, **1**, 3408-3413.
- ⁷ G. Shwarz, I. Hasslauer, D.G. Kurth, *Adv. Colloid Interf. Sci.*, 2014, **207**, 107-120.
- ⁸ E. C. Constable, K. Harris, C. E. Housecroft, M. Neuburger, S. Schaffner, *Chem. Commun.*, **2008**, 5360-5362.
- ⁹ F. S. Han, M. Higuchi, D. G. Kurth, *J. Am. Chem. Soc.*, 2008, **130**, 2073-2081.
- ¹⁰ Y. T. Chan, C. N. Moorefield, M. Soler, G. R. Newkome, *Chem. Eur. J.*, 2010, **16**, 1768-1771.
- ¹¹ S. Schmatloch, U. S. Schubert, *Macromol. Symp.*, 2003, **199**, 483-497.
- ¹² E. C. Constable, *Chem. Soc. Rev.*, 2007, **36**, 246-253.
- ¹³ a) G.D. Storrer, S.B. Colbran, *J. Chem. Soc., Dalton Trans.*, 1996, 2185-2186 ; b) G.D. Storrer, S. B. Colbran, D. C. Craig, *J. Chem. Soc., Dalton Trans.*, 1997, 3011-3028.
- ¹⁴ R. Dobraza, F. Würthner, *Chem. Commun.*, 2002, 1878-1879.

- ¹⁵ V. Stepanenko, M. Stocker, P. Muller, M. Buchner, F. Würthner, *J. Mater. Chem.*, 2009, **19**, 6816-6826.
- ¹⁶ N. Tuccitto, I. Delfanti, V. Torrisi, F. Scandola, C. Chiorboli, V. Stepanenko, F. Würthner, A. Licciardello, *Phys. Chem. Chem. Phys.*, 2009, **11**, 4033-4038.
- ¹⁷ S. C. Yu, C. C. Kwok, W. K. Chan, C. M. Che, *Adv. Mater.*, 2003, **15**, 1643-1647.
- ¹⁸ Y. Y. Chen, Y. T. Tao, H. C. Lin, *Macromolecules*, 2006, **39**, 8559-8566.
- ¹⁹ Y. Y. Chen, H. C. Lin, *Polymer* 2007, **48**, 5268-5278 and *J. Polym. Sci. Pol. Chem.*, 2007, **45**, 3243-3255.
- ²⁰ F. Schlutter, A. Wild, A. Winter, M. D. Hager, A. Baumgaertel, C. Friebe, U. S. Schubert, *Macromolecules*, 2010, **43**, 2759-2771.
- ²¹ A. Gasnier, J. M. Barbe, C. Bucher, F. Denat, J. C. Moutet, E. Saint-Aman, P. Terech, G. Royal, *Inorg. Chem.*, 2008, **47**, 1862-1864.
- ²² A. Gasnier, G. Royal, P. Terech, *Langmuir*, 2009, **25**, 8751-8762.
- ²³ A. Gasnier, J. M. Barbe, C. Bucher, C. Duboc, J. C. Moutet, E. Saint-Aman, P. Terech, G. Royal, *Inorg. Chem.*, 2010, **49**, 2592-2599.
- ²⁴ M. Yan, S. K. P. Velu, G. Royal, P. Terech, *J. Colloid Interf. Sci.*, 2013, **399**, 6-12.
- ²⁵ E. Medlycott, G. Hanan, *Coord. Chem. Rev.*, 2006, **250**, 1763-1782.
- ²⁶ B. Galland, D. Limosin, H. Laguitton-Pasquier, A. Deronzier, *Inorg. Chem. Commun.*, 2002, **5**, 5-8.
- ²⁷ J. Lombard, J. C. Lepretre, J. Chauvin, M.-N. Collomb, A. Deronzier, *Dalton Trans.*, 2008, 658-666.
- ²⁸ J. Lombard, R. Boulaouche, D. A. Jose, J. Chauvin, M.-N. Collomb, A. Deronzier, *Inorg. Chim. Acta*, 2010, **363**, 234-242.
- ²⁹ C. E. Castillo, S. Romain, M. Retegan, J.-C. Lepretre, J. Chauvin, C. Duboc, J. Fortage, A. Deronzier, M.-N. Collomb, *Eur. J. Inorg. Chem.*, 2012, 5485-5499.
- ³⁰ R. Horvath, J. Lombard, J.-C. Lepretre, M.-N. Collomb, A. Deronzier, J. Chauvin, K. Gordon, *Dalton Trans.*, 2013, **42**, 16527-16537.
- ³¹ M.-N. Collomb, A. Deronzier, *Eur. J. Inorg. Chem.* 2009, 2025-2046.
- ³² J. Lombard, J.-C. Lepretre, D. Jouvenot, A. Deronzier, M.-N. Collomb, *New J. Chem.*, 2008, **32**, 1117-1123.
- ³³ K. Gorgy, M.-N. Collomb, J.-C. Lepretre, A. Deronzier, C. Duboc-Toia, S. Menage, M. Fontecave, *Electrochem. Commun.*, 2001, **3**, 686-691.
- ³⁴ A. Deronzier, D. Eloy, P. Jardon, A. Martre, J. C. Moutet, *J. Electroanal. Chem.*, 1998, **453**, 179-185.
- ³⁵ A. Deronzier, J. C. Moutet, D. Zsoldos, *J. Phys. Chem.*, 1994, **98**, 3086-3089.
- ³⁶ J.-A. Spitz, R. Yasukuni, N. Sandeau, M. Takano, J.-J. Vachon, R. Meallet-Renault, R.B. Pansu, *J. Microsc.*, 2008, **229**, 104-114.
- ³⁷ S. Schmatloch, A.M.J. van den Berg, A.S. Alexeev, H. Hofmeier, U.S. Schubert, *Macromolecules*, 2003, **36**, 9943-9949.
- ³⁸ C. M. Elliott, C. J. Baldy, L. M. Nuwaysir, C. L. Wilkins, *Inorg. Chem.*, 1990, **29**, 389-392.

- ³⁹ Y. Lattach, J.-F. Rivera, T. Bamine, A. Deronzier, J.-C. Moutet, *ACS Appl. Mater. Interfaces*, 2014, **6**, 12852-12859.
- ⁴⁰ S. Liatard, J. Chauvin, F. Balestro, D. Jouvenot, F. Loiseau, A. Deronzier, *Langmuir*, 2012, **28**, 10916-10924.
- ⁴¹ R. H. Schmehl, R. A. Auerbach, W. F. Wacholtz, C. M. Elliott, R. A. Freitag, J. W. Merkert, *Inorg. Chem.*, 1986, **25**, 2440-2445.
- ⁴² H. Wolpher, P. Huang, M. Borgstrom, J. Bergquist, S. Styring, L. Sun, B. Akermark, *Catal. Today*, 2004, **98**, 529-536.
- ⁴³ L. M. Dupray, T. J. Meyer, *Inorg. Chem.*, 1996, **35**, 6299-6307.
- ⁴⁴ H. Laguitton-Pasquier, A. Martre, A. Deronzier, *J. Phys. Chem. B.*, 2001, **105**, 4801-4809.
- ⁴⁵ Y. Yamamoto, S. Sawa, Y. Funada, T. Morimoto, M. Falkenstrom, H. Miyasaka, S. Shishido, T. Ozeki, K. Koike, O. Ishitani, *J. Am. Chem. Soc.*, 2008, **130**, 14659-14674.
- ⁴⁶ A. Winter, C. Friebe, M. D. Hager, U. S. Schubert, *Eur.J. Org. Chem.*, 2009, 801-809.
- ⁴⁷ H. Cano-Yelo, A. Deronzier, *J. Chem. Soc., Faraday Trans. 1*, 1984, **80**, 3011-3019 and *Tetrahedron Lett.*, 1984, **25**, 5517-5520.
- ⁴⁸ A. Deronzier, P. Jardon, A. Martre, J.-C. Moutet, C. Santato, V. Balzani, A. Credi, F. Paolucci, S. Roffia, *New J. Chem.*, 1998, **22**, 33-37.

Table 1. Redox potentials of $[M(\text{tolyl-tpy})_2]^{2+}$ ($M = \text{Fe}^{2+}, \text{Zn}^{2+}$), $[\text{Ru}(\text{bpy})_2(\text{L2})]^{2+}$ and of their corresponding $[\{\text{Ru}^{\text{II}}-\text{M}^{\text{II}}\}_n]^{4n+}$ coordination polymer in deoxygenated $\text{CH}_3\text{CN} + 0.1 \text{ M} [\text{Bu}_4\text{N}]\text{ClO}_4$ (scan rate of 100 mV s^{-1}). $E_{1/2}(\text{V})(\Delta E_p/\text{mV})$ vs Ag/Ag^+ (AgNO_3 10 mM in $\text{CH}_3\text{CN} + 0.1 \text{ M} [\text{Bu}_4\text{N}]\text{ClO}_4$).

Complexes	Oxidation processes		Ligand centered reduction processes			
	$\text{M}^{\text{III}}/\text{M}^{\text{II}}$	$\text{Ru}^{\text{III}}/\text{Ru}^{\text{II}}$				
$[\text{Fe}(\text{tolyl-tpy})_2]^{2+}$	0.76(60)	-	-1.54(60)	-1.65(60)		
$[\text{Zn}(\text{tolyl-tpy})_2]^{2+}$	-	-	-1.56	-1.72		
$[\text{Ru}^{\text{II}}(\text{bpy})_2(\text{L2})]^{2+}$		0.92(60)	-1.67(60)	-1.87(70)	-2.19(100)	
$[\{\text{Ru}^{\text{II}}-\text{Fe}^{\text{II}}\}_n]^{4n+}$	0.75(40)	0.91(40)	-1.52 ^a (80)	-1.61(60)	-1.80(50)	-2.20 ^b
$[\{\text{Ru}^{\text{II}}-\text{Zn}^{\text{II}}\}_n]^{4n+}$	-	0.91(20)	-1.52 ^a	-1.64(40)	-1.82(80)	-2.30 ^b

^a Shoulder in front of the next reduction wave.

^b This value cannot be accurately measured since the wave is strongly distorted by adsorption of the reduction product on the electrode surface.

Table 2. UV-visible and emission properties of $[M(\text{tolyl-tpy})_2]^{2+}$ ($M = \text{Fe}^{2+}, \text{Zn}^{2+}$) $[\text{Ru}(\text{bpy})_2(\text{L2})]^{2+}$ and the corresponding $[\{\text{Ru}^{\text{II}}-\text{M}^{\text{II}}\}_n]^{4n+}$ coordination polymer in deoxygenated CH_3CN

Complexes	$\lambda_{\text{abs}}^{\text{max}} / \text{nm}$ ($\epsilon / \text{M}^{-1} \text{cm}^{-1}$)	$\lambda_{\text{em}}^{\text{max}}$ nm	ϕ	luminescence lifetime τ_1 ns (%); τ_2 ns (%)
$[\text{Fe}(\text{tolyl-tpy})_2]^{2+, 27}$	285(68200), 320(62800), 567(25900)			
$[\text{Zn}(\text{tolyl-tpy})_2]^{2+}$	285(68000), 313(54800), 54600(54600)			
$[\text{Ru}(\text{bpy})_2(\text{L2})]^{2+, 26}$	288(96700), 455(13000)	609	0.046	$\tau = 1014$ ns
$[\{\text{Ru}^{\text{II}}-\text{Fe}^{\text{II}}\}_n]^{4n+}$	456(17200), 568(21200)	616	0.002	3.2 (98%); 690 (2%)
$[\{\text{Ru}^{\text{II}}-\text{Zn}^{\text{II}}\}_n]^{4n+}$	287(130200), 455(13000)	614	0.054	15 (88%); 720 (12%)

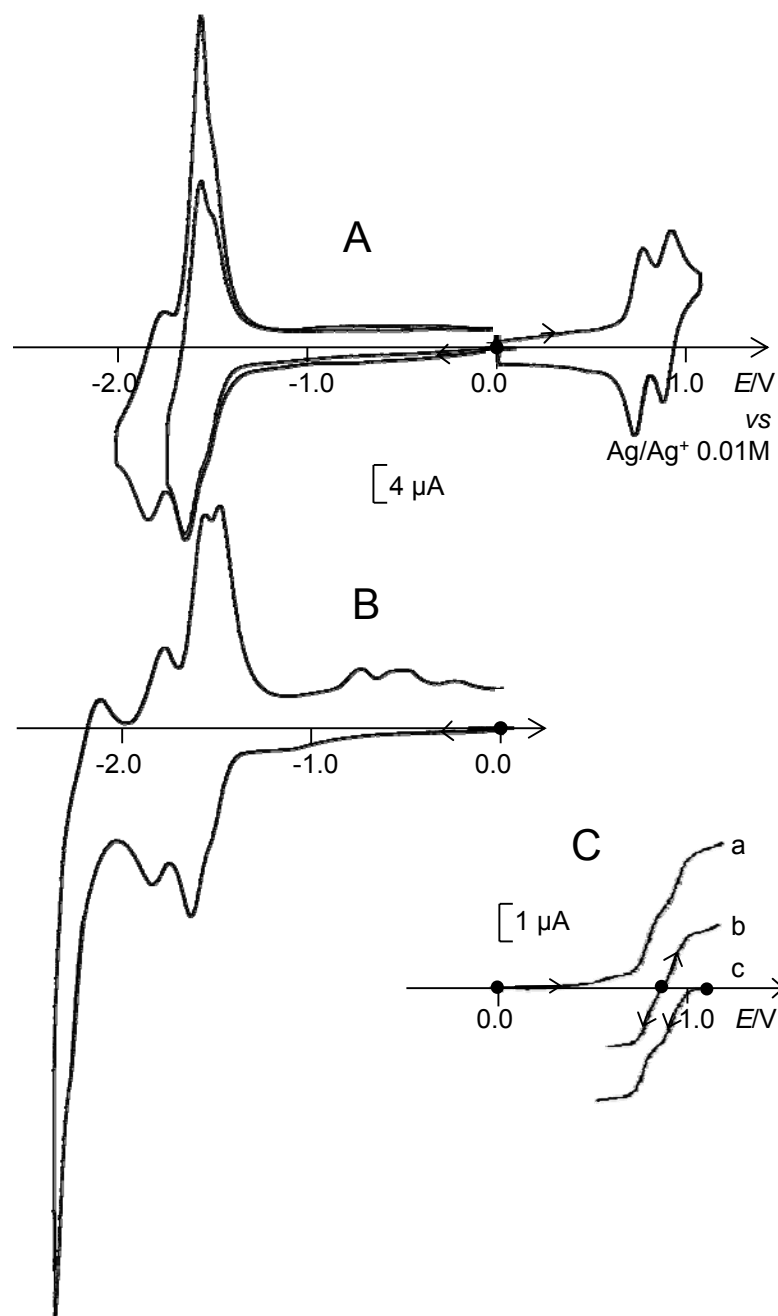


Figure 1: (A, B) Cyclic voltammograms in $\text{CH}_3\text{CN} + 0.05 \text{ M } [\text{Bu}_4\text{N}]\text{BF}_4$ at a Pt electrode of a 0.23 mM solution of $[\{\text{Ru}^{\text{II}}-\text{Fe}^{\text{II}}\}_n]^{4n+}$ at different scan range; scan rate: 100 mV s^{-1} . (C) Voltammograms at a rotating disk electrode (RDE) of the same solution at a Pt electrode; rotation rate $\omega = 600 \text{ rot min}^{-1}$; scan rate: 10 mV s^{-1} , (a) initial solution, (b) after exhaustive electrolysis at $+0.90 \text{ V}$, (c) after exhaustive electrolysis at $+1.05 \text{ V}$.

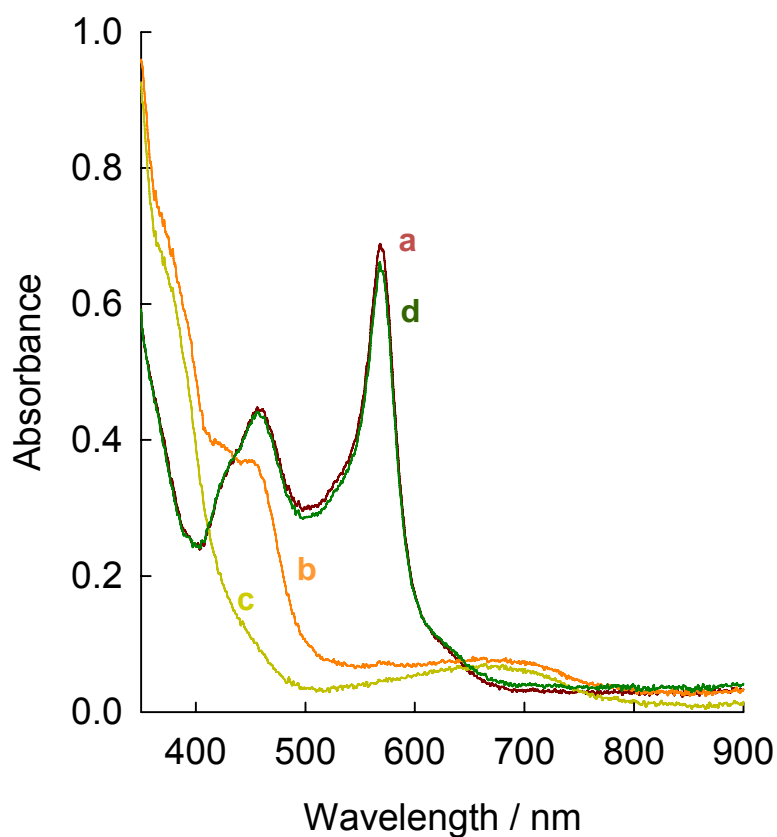


Figure 2: Absorption spectra of a 0.24 mM solution of $[\{\text{Ru}^{\text{II}}\text{-Fe}^{\text{II}}\}_n]^{4n+}$ in $\text{CH}_3\text{CN} + 0.05 \text{ M } [\text{Bu}_4\text{N}]\text{BF}_4$: (a) initial solution; (b) after exhaustive electrolysis at +0.90 V; (c) after exhaustive electrolysis at +1.05 V; (d) after exhaustive electrolysis at +0.60 V; $l = 1 \text{ mm}$.

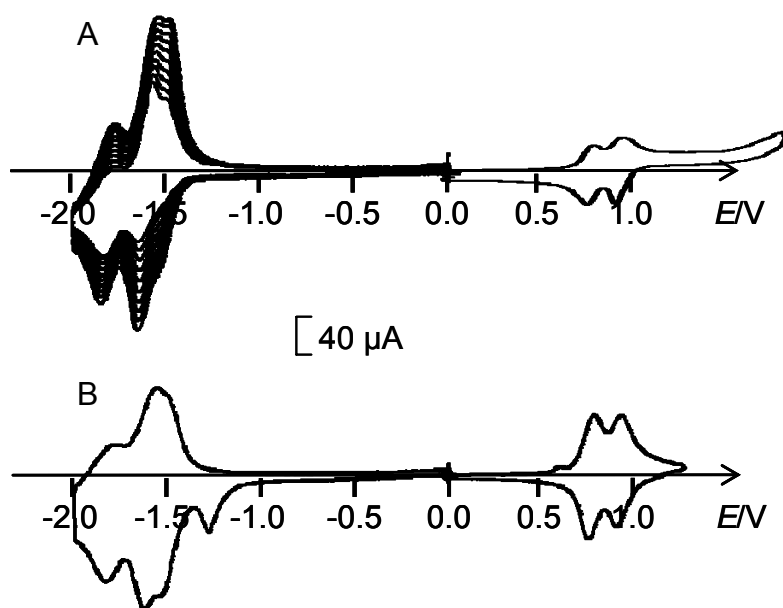


Figure 3: (A) Elaboration of a modified electrode $\text{Pt}/[\{\text{Ru}^{\text{II}}\text{-Fe}^{\text{II}}\}_n]^{4n+}$ by 10 successive potential scans between 0 and -2.0 V from a solution of $[\{\text{Ru}^{\text{II}}\text{-Fe}^{\text{II}}\}_n]^{4n+}$ (1.1 mM) in $\text{CH}_3\text{CN} + 0.1 \text{ M } [\text{Bu}_4\text{N}]\text{ClO}_4$, (B) Cyclic voltammograms of the resulting modified electrode prepared in (A) after transfer in $\text{CH}_3\text{CN} + 0.1 \text{ M } [\text{Bu}_4\text{N}]\text{ClO}_4$, $\Gamma = 6.3 \times 10^{-9} \text{ mol/cm}^2$; scan rate 100 mV s^{-1} .

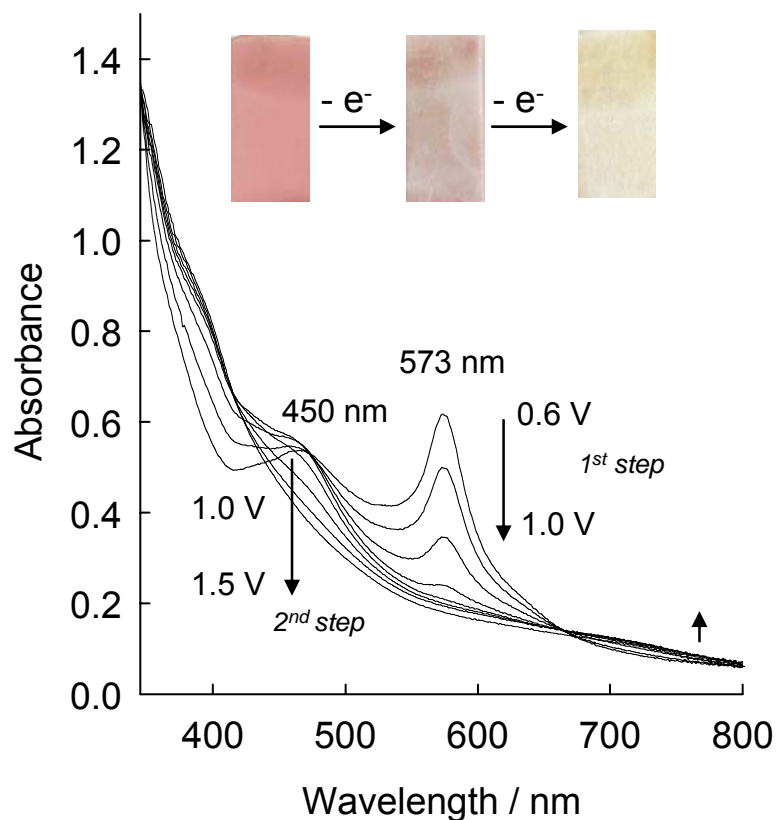


Figure 4: Absorbance spectra of a $[\{\text{Ru}^{\text{II}}\text{-Fe}^{\text{II}}\}_n]^{4n+}$ film deposited on an ITO electrode ($\Gamma = 5.83 \times 10^{-8} \text{ mol/cm}^2$) recorded in $\text{CH}_3\text{CN} + 0.1 \text{ M } [\text{Bu}_4\text{N}]\text{ClO}_4$, during the cyclage between +0.6 and +1.5 V; scan rate: 5 mV s^{-1} . In a first step, the band at 573 nm decrease until its complete disappearance (formation of $\text{ITO}/[\{\text{Ru}^{\text{II}}\text{-Fe}^{\text{III}}\}_n]^{5n+}$); in a second step the band at 450 nm decrease (formation of $\text{ITO}/[\{\text{Ru}^{\text{III}}\text{-Fe}^{\text{III}}\}_n]^{6n+}$).

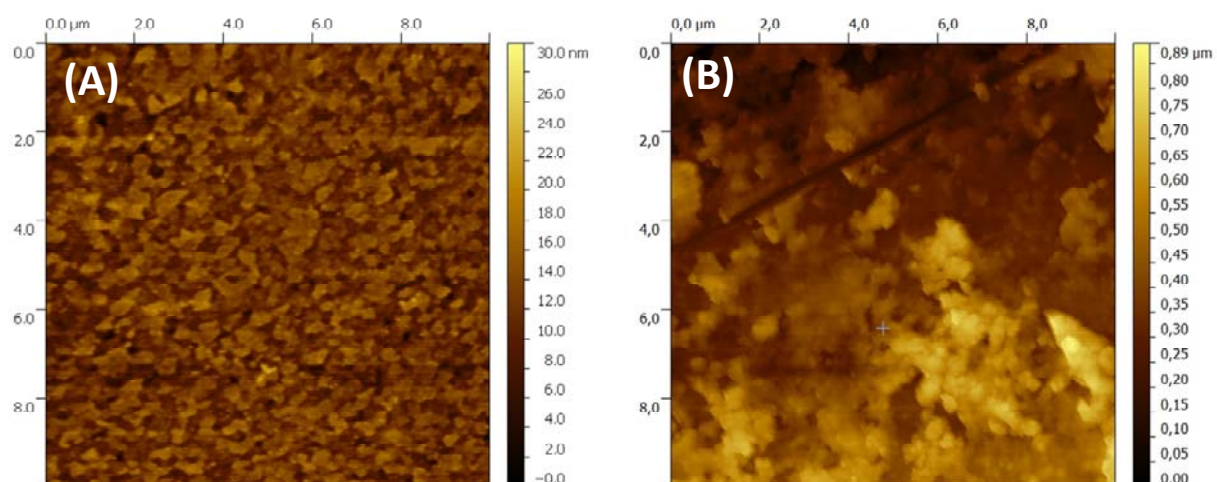


Figure 5: AFM images in tapping mode of an ITO naked electrode (A) and ITO coated with a $([\text{Ru}^{\text{II}}\text{-Fe}^{\text{II}}]_n)^{4n+}$ thin film ($\Gamma = 5.83 \times 10^{-8} \text{ mol/cm}^2$) (B).

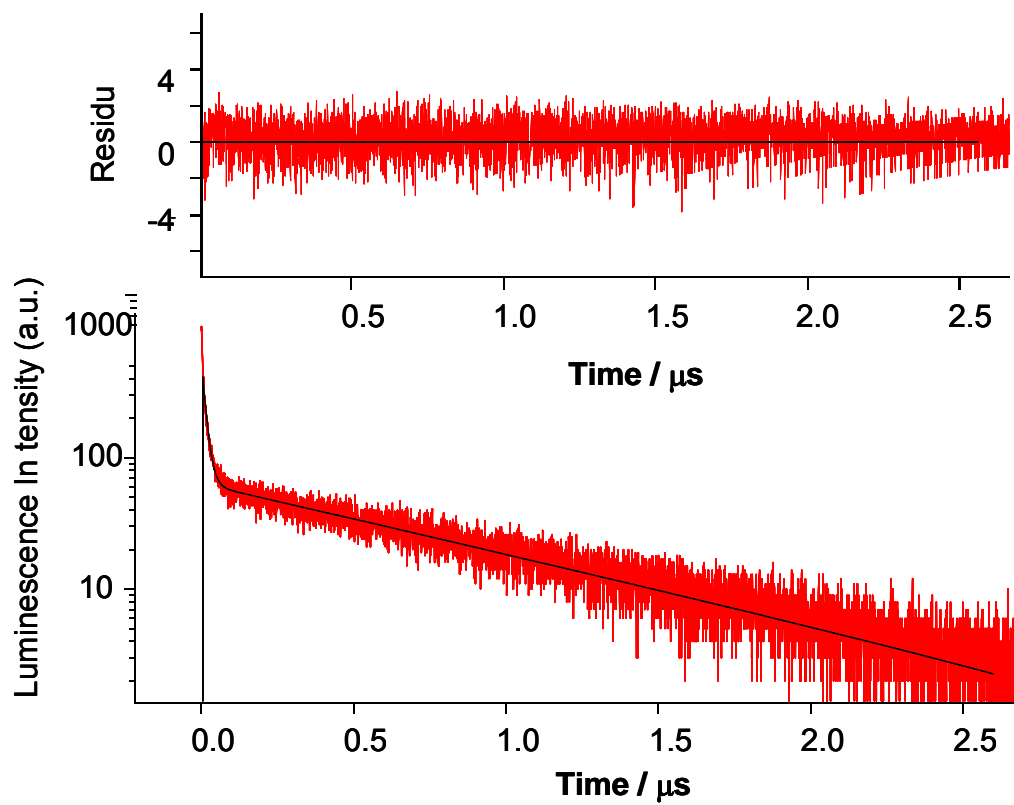


Figure 6: Luminescence decay of $[\{\text{Ru}^{\text{II}}\text{-Zn}^{\text{II}}\}_n]^{4n+}$ (0.015 mM) in deoxygenated CH_3CN upon excitation at 400 nm. The decay is fitted by a bi-exponential function according to equation 7.

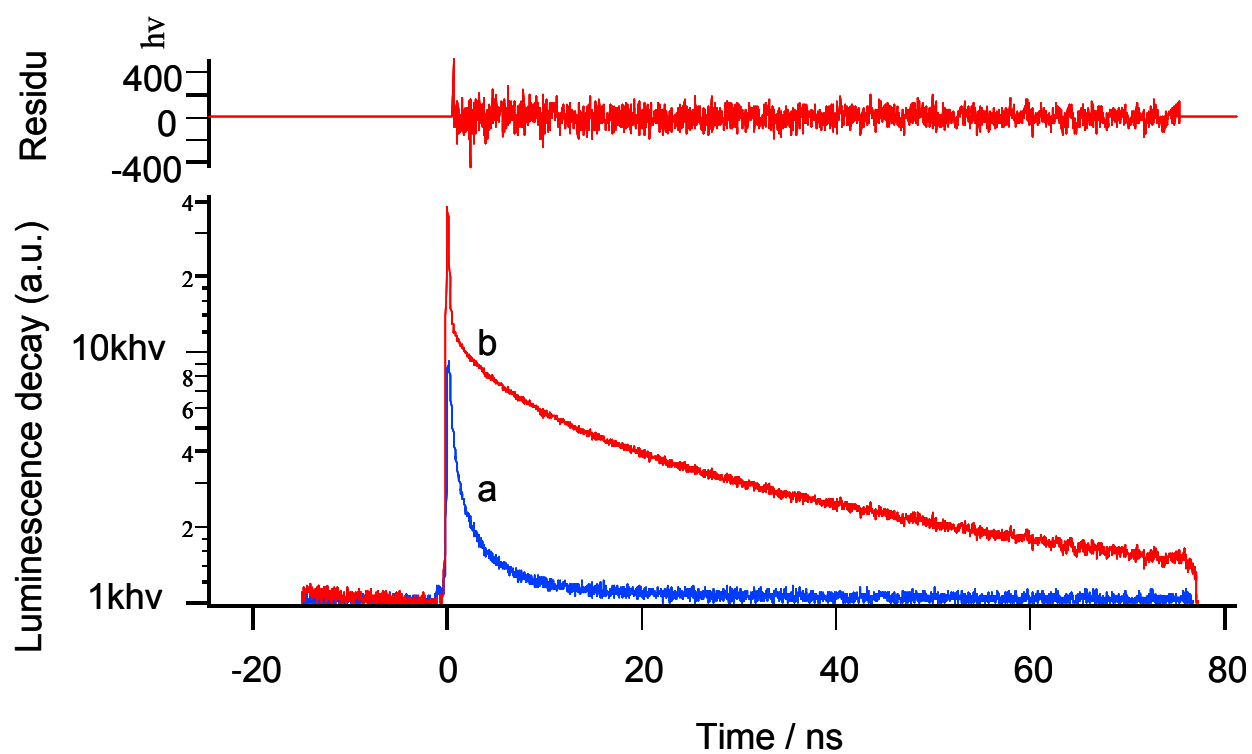


Figure 7: Luminescence decay upon excitation at 343 nm of a naked ITO electrode (a) and a $[\{\text{Ru}^{\text{II}}\text{-Zn}^{\text{II}}\}_n]^{4n+}$ film deposited on ITO ($\Gamma = 3.9 \times 10^{-8} \text{ mol/cm}^2$) (b). The luminescence decay in (b) is fitted by a stretched exponential function according to equation 9 with $\beta = 0.4$ and $\tau = 9.5 \text{ ns}$.

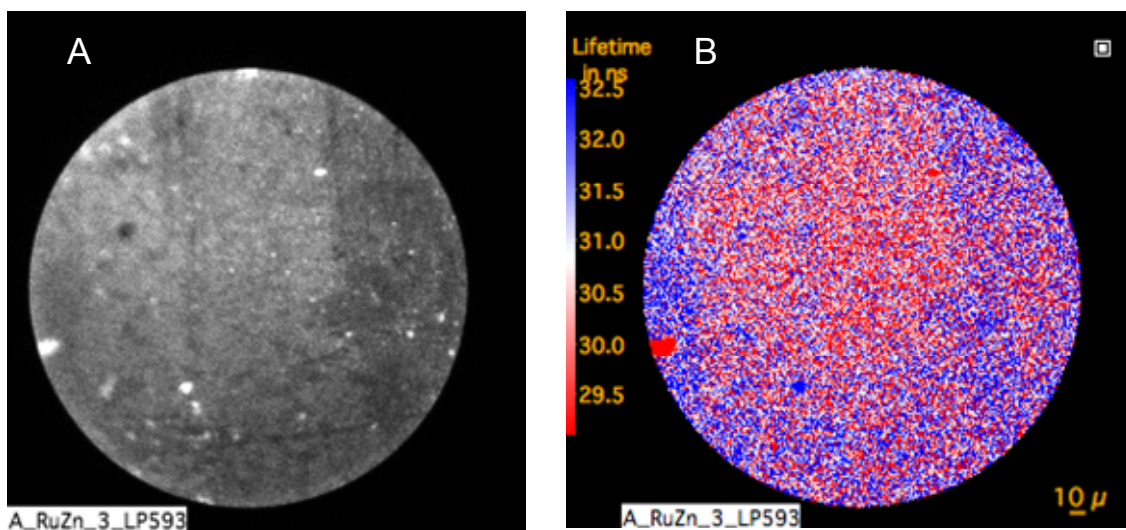


Figure 8: Emission properties of a $[\{\text{Ru}^{\text{II}}\text{-Zn}^{\text{II}}\}_n]^{4n+}$ film deposited on ITO ($\Gamma = 3.9 \times 10^{-8}$ mol/cm²) recorded upon excitation at 343 nm. (A) Steady state emission and (B) Emission decay map.

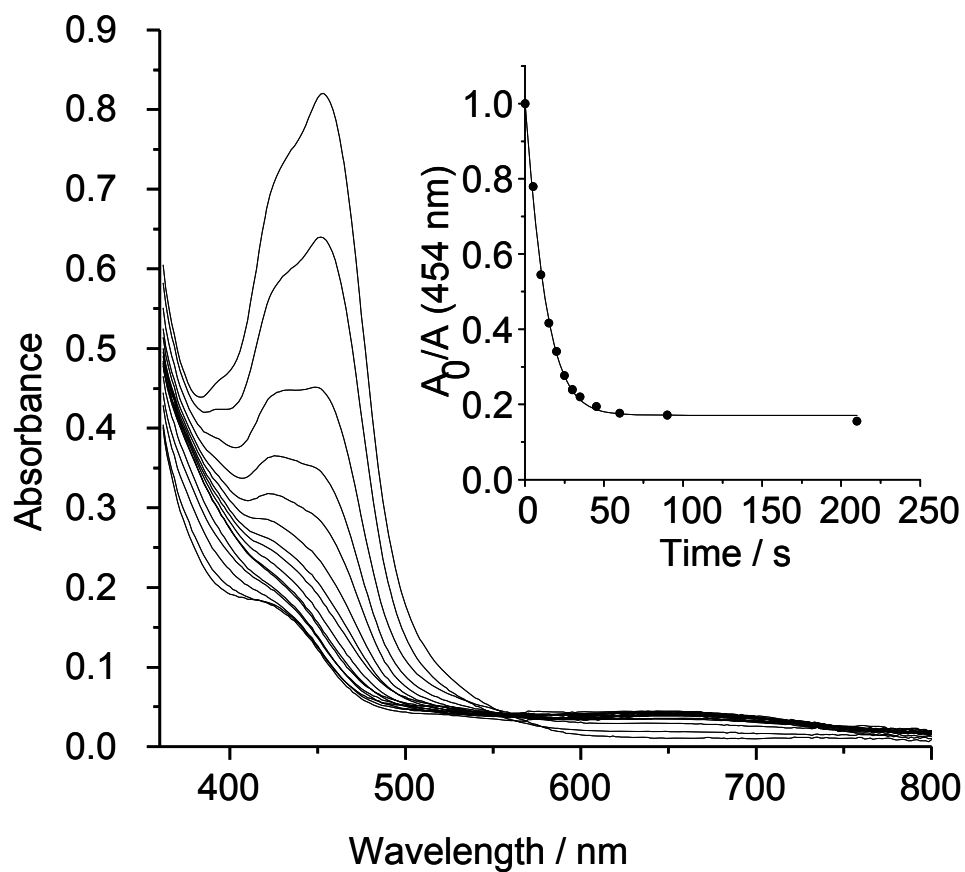


Figure 9: Visible absorption changes under visible irradiation of a mixture of $[\text{Ru}^{\text{II}}-\text{Zn}^{\text{II}}]^{4n+}$ (0.05 mM) and ArN_2^+ (15 mM) in CH_3CN , $l = 1$ cm: photogeneration of $[\text{Ru}^{\text{III}}-\text{Zn}^{\text{II}}]^{5n+}$. Inset: Evolution of the absorbance at 454 nm

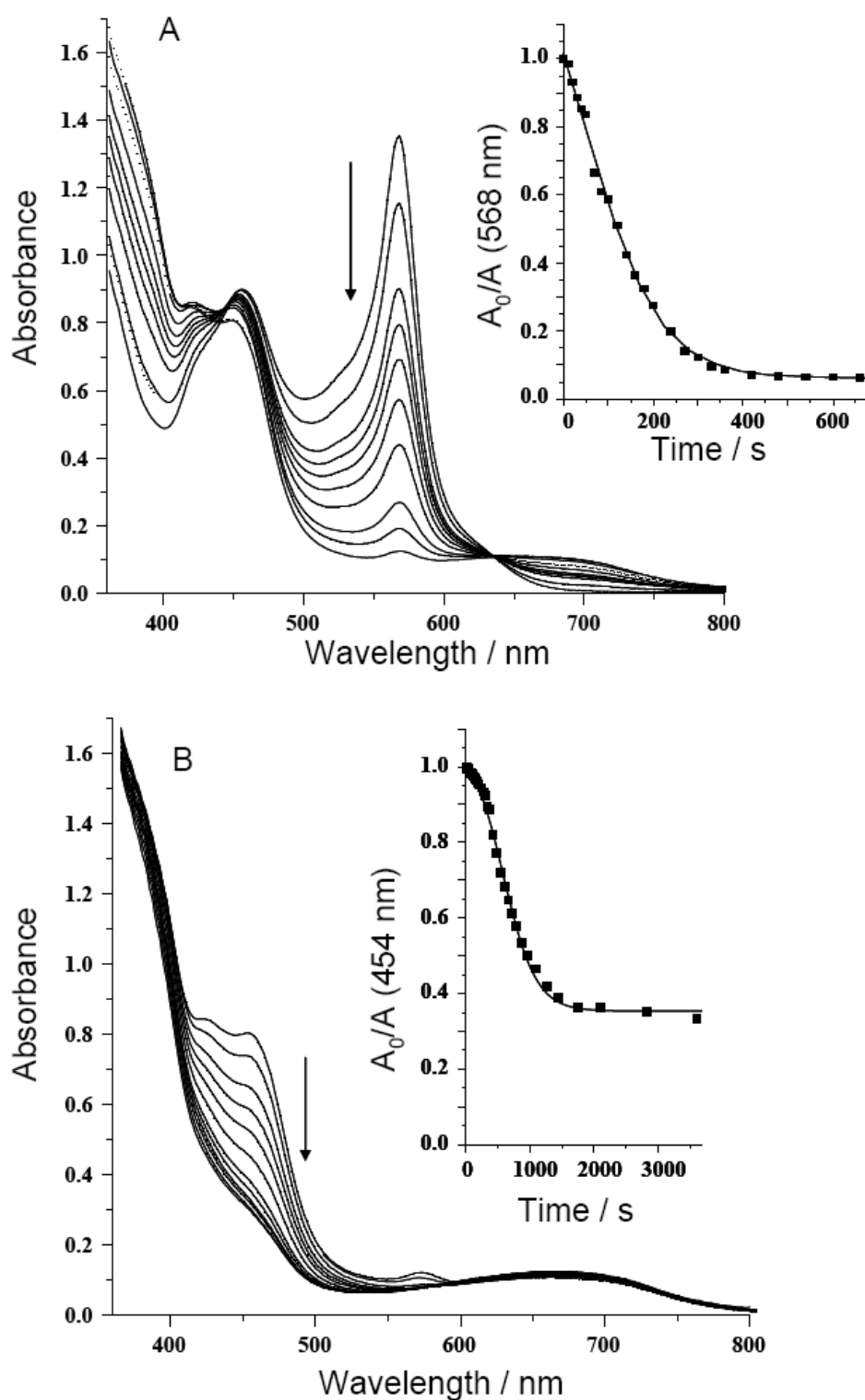


Figure 10: Visible absorption changes under visible irradiation of a mixture of $[\{\text{Ru}^{\text{II}}\text{-Fe}^{\text{II}}\}_n]^{4n+}$ (0.06 mM) and ArN_2^+ (15 mM) in CH_3CN , $l = 1$ cm. (A) Photogeneration of $[\{\text{Ru}^{\text{II}}\text{-Fe}^{\text{III}}\}_n]^{5n+}$, inset: evolution of the absorbance at 568 nm; (B) Photogeneration of $[\{\text{Ru}^{\text{III}}\text{-Fe}^{\text{III}}\}_n]^{6n+}$, inset: evolution of the absorbance at 454 nm.

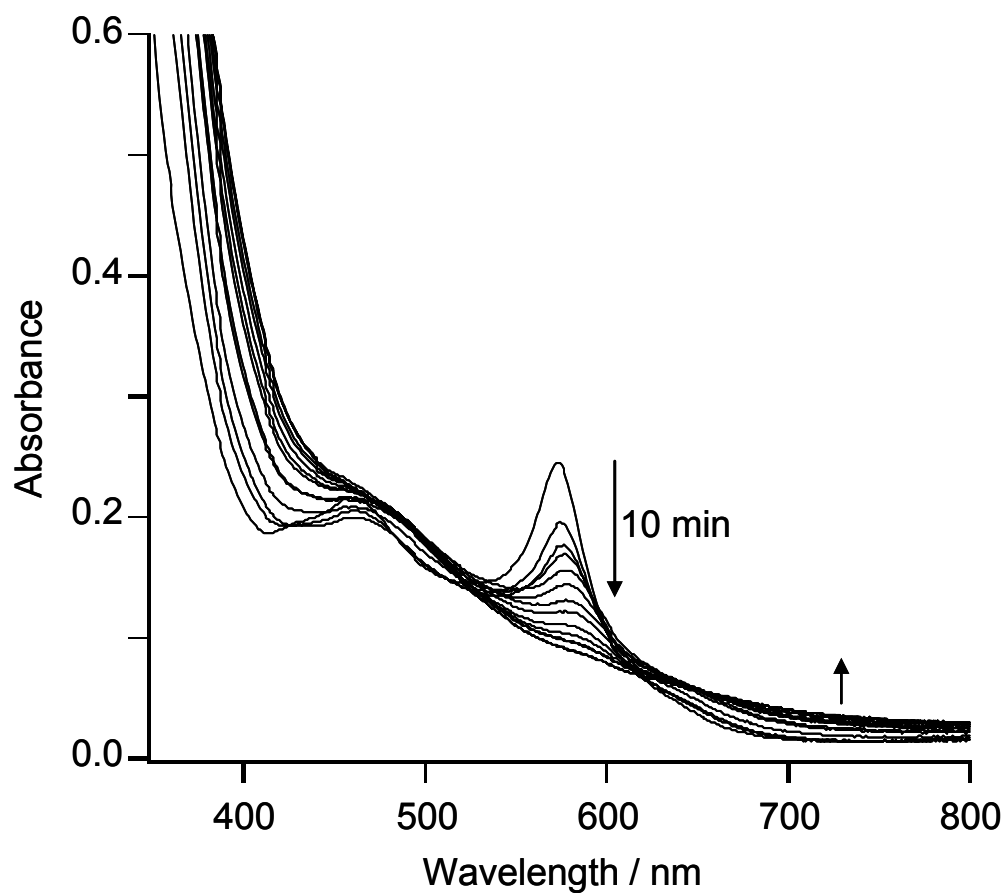


Figure 11: Visible absorption changes under visible irradiation of a [$\{\text{Ru}^{\text{II}}\text{-Fe}^{\text{II}}\}_n\}^{4n+}$] film deposited on ITO ($\Gamma = 3.04 \times 10^{-8} \text{ mol/cm}^2$) in $\text{CH}_3\text{CN} + 0.1 \text{ M } [\text{Bu}_4\text{N}]\text{ClO}_4$ in presence of ArN_2^+ (15 mM).